Infrared Spectra and Density Functional Calculations of $CH_2{=}MHX$ and $CH{\equiv}MH_2X$ Complexes Prepared in Reactions of Methyl Halides with Mo and W Atoms

Han-Gook Cho and Lester Andrews*

Department of Chemistry, University of Incheon, 177 Dohwa-dong, Nam-ku, Incheon, 402-749, South Korea, and Department of Chemistry, University of Virginia, P.O. Box 400319, Charlottesville, Virginia 22904-4319

Received: June 29, 2006; In Final Form: August 23, 2006

The simple methylidene and methylidyne complexes ($CH_2{=}MHX$ and $CH{\equiv}MH_2X$; X = F, Cl, Br, and I) are prepared in reactions of laser-ablated Mo and W atoms with the methyl halides and investigated by matrix infrared spectroscopy and density functional theory calculations. These complex structures are photoreversible: visible irradiation converts the methylidene complex to the methylidyne complex, and UV irradiation reverses this effect via α-hydrogen migration. While the higher oxidation state complexes are readily formed regardless of halogen size, the Mo methylidyne complex is relatively less favored with increasing halogen size, and the W complex shows the opposite tendency. The group 6 metal methylidenes are predicted to have the most agostically distorted structures among the early transition-metal methylidenes. The computed carbon−metal bond shortens with increasing halogen size for both the methylidene and methylidyne complexes. Harmonic and anharmonic frequencies computed by DFT converge on the experimental values and thus provide support for the identification of these new Mo and W complexes.

Introduction

Since their discovery in 1970s,[1] the interest in high-oxidation-state alkylidene ($M{=}CR_1R_2$) and alkylidyne ($M{\equiv}CR$) complexes has grown dramatically, owing to the catalytic activities of the complexes to metathesis of alkenes, alkynes, and cyclic compounds.[2] The high-oxidation-state complexes, often called Schrock carbenes and carbynes, are also used as C−H activating agents.[3] Methylidene and methylidyne complexes, the simplest forms of metal alkylidenes and alkylidynes, provide ideal model systems to study the effects of ligands and substituent modifications. Particularly, the high-oxidation-state complexes derived from simple halomethanes and methane have been prepared by direct metal atom reactions and characterized by infrared spectroscopy and density functional calculations.[4−10]

Siegbahn and Blomberg theoretically investigated activation of the C−H bond by second-row transition-metal atoms and the effects of halogen coordination to the metal atom.[11] Gordon et al. examined the geometries and vibrational characteristics of the simple methylidene complexes of groups 5 and 6 metals.[12] Hehre also studied groups 5 and 6 transition-metal methylidene complexes and examined the rotational barrieriers.[13] It is well-known that many alkylidene complexes show agostic distortion, which is traditionally explained as coordination of a C−H bond near the electron-deficient transition-metal atom. Scherer and McGrady, on the other hand, suggested in a recent study that the distortion originates from negative hyperconjugation of the carbon−metal bond and therefore includes structural rearrangement around the bond as well as inclination of the hydrogen atom.[15] More recently, von Frantzius et al. investigated the agostic interaction of Ti and group 6 metal alkylidenes and estimated that the interaction energy was in the range of a typical hydrogen bond (≤10 kcal/mol).[16]

Reactions of groups 4, 5, and 6 transition metals with methane and methyl halides have been carried out recently in our laboratories.[4−10] Various insertion complexes have been prepared, and many of them can be considered small model systems for much larger high-oxidation-state complexes.[2] The small complexes often possess agostically distorted structures and show interesting matrix effects and remarkable photochemistry, including persistent photoreversibilities and dramatic product increases. Progressive variations in reactivities of the early transition metals are found by moving horizontally and vertically in the periodic table. Heavy group 6 metals (Mo and W) yield triple-bonded complexes with CH_3F and CH_4 as well as single- and double-bonded products, while Cr forms only single-bonded insertion complexes.[6,9]

In this study, reactions of Mo and W with methyl halides are carried out, and the ligand effects for the high-oxidation-state complexes are examined. Photoreversible pairs of methylidene and methylidyne complexes are readily formed regardless of halogen size, and the methylidene complexes are most agostically distorted among the groups 3−6 metal methylidenes formed from later-ablated metals and methyl halides. Products are identified by isotopic substitutions and complementary DFT calculations.

Experimental and Computation Methods

Laser-ablated Mo and W atoms (Johnson-Matthey) were reacted with CH_3X isotopomers (CH_3Cl, CH_3Br, CD_3Br (Cambridge Isotopic Laboratories, 99%), CH_3I, CD_3I (Aldrich, 99.5%), and CD_3Cl (synthesized from CD_3Br and $HgCl_2$),) in excess argon during condensation at 8 K using a closed-cycle He refrigerator (Air Products HC-2). The methods are previously described in detail elsewhere.[17] Concentrations of gas mixtures are typically 0.2−1.0% in argon. After reaction, infrared spectra were recorded at a resolution of 0.5 cm^{-1} using a Nicolet 550 spectrometer with an HgCdTe low-frequency response detector. Samples were later irradiated by a mercury arc lamp (175 W) with a combination of optical filters, were annealed, and more spectra were recorded.

* To whom correspondence should be addressed. E-mail: lsa@virginia.edu.

10.1021/jp064085n CCC: $33.50
Published on Web 11/16/2006

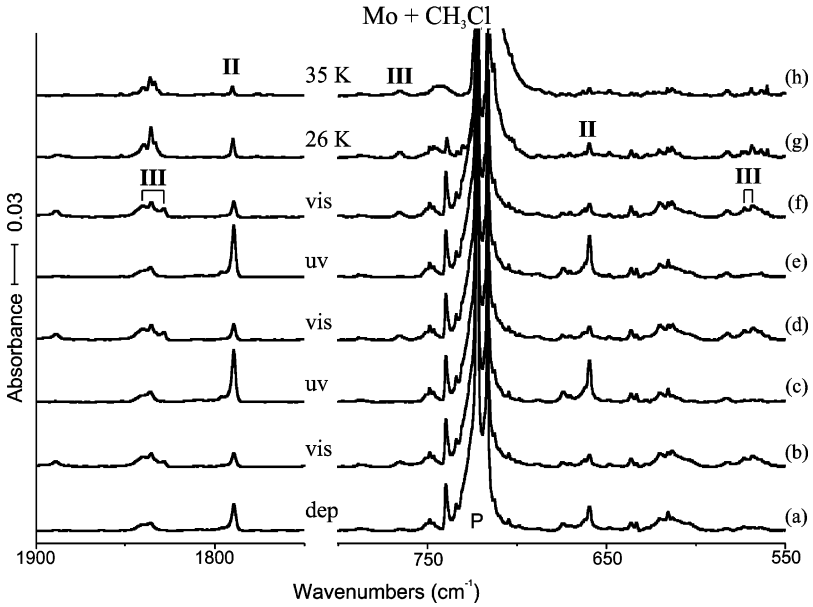

Figure 1. Infrared spectra in the regions 1950−1750 and 800−550 cm^{-1} for laser-ablated Mo atoms codeposited with CH_3Cl in excess argon at 8 K and their variation. (a) Mo + 0.5% CH_3Cl in Ar codeposited for 1 h. (b) After broadband photolysis with a filter ($\lambda > 420$ nm) for 15 min. (c) After broadband photolysis with a filter ($240 < \lambda < 380$ nm) for 30 min. (d) After broadband photolysis with a filter ($\lambda > 420$ nm) for 15 min. (e) After broadband photolysis with a filter ($240 < \lambda < 380$ nm) for 15 min. (f) After broadband photolysis with a filter ($\lambda > 420$ nm) for 15 min. (g) After annealing to 26 K. (h) After annealing to 35 K. II and III denote the product absorption groups and P indicates precursor absorption.

TABLE 1: Frequencies of Product Absorptions Observed from Reactions of Methyl Halides with Mo Atoms in Excess Argon[a]

group	CH_3F	CD_3F	$^{13}CH_3F$	CH_3Cl	CD_3Cl	CH_3Br	CD_3Br	CH_3I	CD_3I	description
I	589.3	589.0	589.3							A′ Mo−X str.
	441.1									A′ C−Mo str.
II	1797.7	1292.1	1797.7	1789.5	1286.5	1787.3	1284.9	1783.7	1281.5	A′ Mo−H str.
	824.0	737.2	813.9	847.7, 834.8	742.5	845.7, 831.9	737.7	820.7	711.4	A′ C═Mo str,
	801.0	620.0	787.2		605.1					A′ CMoH bend
	675.4	531.2	670.6	659.4	515.5	654.5	509.8	649.5	512.2	A″ CH_2 wag
	642.5	654.3	642.0							A′ Mo−X str.
III	1844.8	1330.5	1844.7	1840.7	1325.8	1843.7	1327.2	1845.5	1317.1	A″ MoH_2 str.
		1322.1		1835.8	1315.7	1831.2	1312.5	1825.1	1306.5	A′ MoH_2 str.
	769.0	675.0	769.0	765.8	568.2	752.3				A′ MoH_2 bend.
	715.8	552.2	711.4	*b*	561.0	714.9	552.2			A′ MoH_2 wag
	557.4		556.9	572.8		569.0				A′ MoCH bend
	571.6		571.6	568.2		562.4				A” MoH_2 deform

[a] All frequencies are in cm^{-1}. Description gives major coordinate. CH_3F data from ref 6. [b] Overlapped by precursor band.

Complementary density functional theory (DFT) calculations were carried out using the *Gaussian03* package,[18] B3LYP density functional,[19] 6-311++G(3df,3pd) basis sets[20] for C, H, F, Cl, and Br, and SDD pseudopotential and basis set[21] for Mo, W, and I to provide a consistent set of harmonic vibrational frequencies for the reaction products. Geometries were fully relaxed during optimization, and the optimized geometry was confirmed by vibrational analysis. Additional BPW91 calculations were performed for the reaction products to support the B3LYP results. All vibrational frequencies were calculated analytically. In calculation of the binding energy of a metal complex, the zero-point energy is included. Tables S1, S2, and S3 (Supporting Information) summarize geometrical parameters and physical constants calculated for the optimized product complexes. As in previous work,[4−10] different spin states were optimized for each structure, and the states reported in the tables are the ground states.

Electronic structure calculations of Mo and W complexes pose a difficult theoretical problem, and DFT provides a good approximation for structures, energies, and vibrational frequencies to support the experimental work.[22] Calculated harmonic frequencies (unscaled) are given for the gaseous species and compared to frequencies measured in a solid argon matrix, which is expected to red-shift the frequencies about 1% from gas-phase values.[23] In the case of FeH_2, the only transition-metal dihydride with a known gas-phase stretching frequency (1674.72 cm^{-1}), this linear quintet molecule antisymmetric mode red-shifts 14 cm^{-1} in solid argon.[24,25] We also compare anharmonic frequencies calculated as described by Barone[26] using *Gaussian03* and B3LYP with the observed absorptions and the calculated harmonic frequencies for our new product molecules.

Results and Discussion

Reactions of Mo and W with methyl halide isotopomers were carried out, and the observed vibrational characteristics and their variations upon photolysis and annealing are compared with frequencies calculated by density functional theory.

Mo + CH_3Cl. The IR spectra in the regions 1740−1640 and 800−620 cm^{-1} from reaction of laser-ablated Mo atoms with CH_3Cl are shown in Figure 1, which includes the original spectra with 0.5% CH_3Cl (a) and their variations upon photolysis and annealing (b−h). Two sets of product absorptions marked II and III are grouped on the basis of their behaviors upon photolysis and annealing as listed in Table 1. Figure 1 clearly

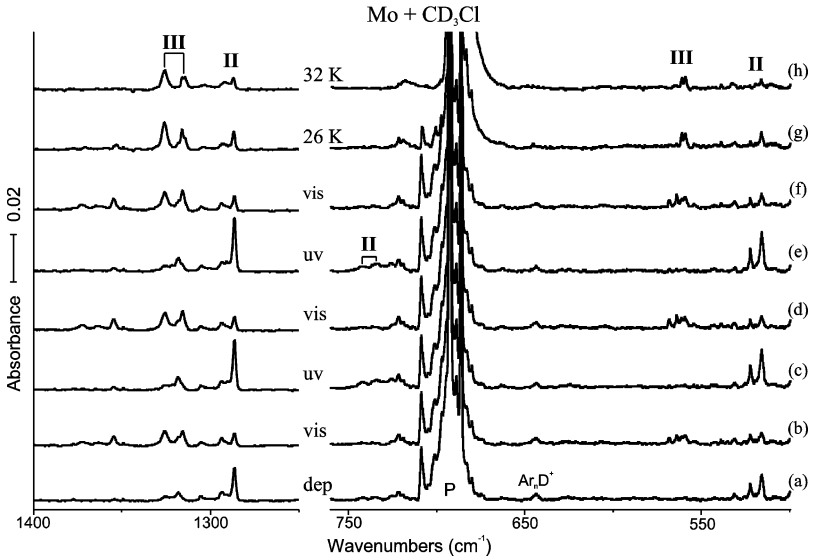

Figure 2. Infrared spectra in the regions 1400−1250 and 760−500 cm^{-1} for laser-ablated Mo atoms codeposited with CD_3Cl in excess argon at 8 K and their variation. ((a) Mo + 0.5% CD_3Cl in Ar codeposited for 1 h. (b) After broadband photolysis with a filter ($\lambda > 420$ nm) for 15 min. (c) After broadband photolysis with a filter ($240 < \lambda < 380$ nm) for 15 min. (d) After broadband photolysis with a filter ($\lambda > 420$ nm) for 15 min. (e) After broadband photolysis with a filter ($240 < \lambda < 380$ nm) for 15 min. (f) After broadband photolysis with a filter ($\lambda > 420$ nm) for 15 min. (g) After annealing to 26 K. (h) After annealing to 32 K. II and III denote the product absorption groups and P indicates precursor absorption.

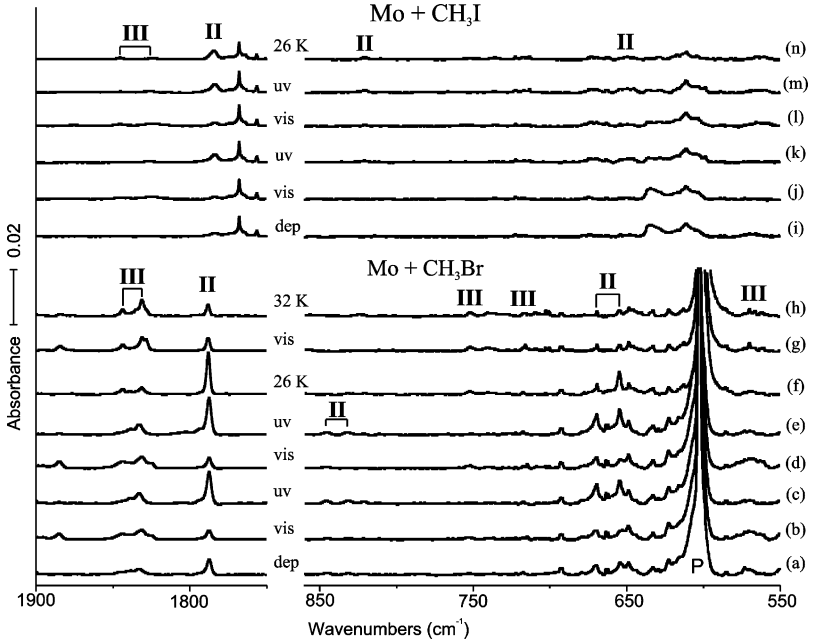

Figure 3. Infrared spectra in the regions 1950−1750 and 860−550 cm^{-1} for laser-ablated Mo atoms codeposited with CH_3Br and CH_3I in excess argon at 8 K and their variations. (a) Mo + 0.5% CH_3Br in Ar codeposited for 1 h. (b) After broadband photolysis with a filter ($\lambda > 420$ nm) for 15 min. (c) After broadband photolysis with a filter ($240 < \lambda < 380$ nm) for 15 min. (d) After broadband photolysis with a filter ($\lambda > 420$ nm) for 15 min. (e) After broadband photolysis with a filter ($240 < \lambda < 380$ nm) for 15 min. (f) After annealing to 26 K. (g) After broadband photolysis with a filter ($\lambda > 420$ nm) for 15 min. (h) After annealing to 32 K. (i) Mo + 1.0% CH_3I in Ar codeposited for 1 h. (j) After broadband photolysis with a filter ($\lambda > 420$ nm) for 20 min. (k) After broadband photolysis with a filter ($240 < \lambda < 380$ nm) for 20 min. (l) After broadband photolysis with a filter ($\lambda > 420$ nm) for 20 min. (m) After broadband photolysis with a filter ($240 < \lambda < 380$ nm) for 20 min. (n) After annealing to 26 K. II and III denote the product absorption groups and P indicates precursor absorption.

shows that the absorptions marked II and III are photoreversible; an increase of one set of absorptions upon photolysis is accompanied with a decrease of the other set of absorptions. The absorptions marked II decrease upon visible ($\lambda > 420$ nm) photolysis, while the absorptions marked III increase. UV ($240 < \lambda < 380$ nm) irradiation reverses the effect. During the subsequent process of stepwise annealing, the absorptions sharpen and ultimately decrease.

The III absorptions are relatively weaker in the original spectra after deposition, but they increase more than 3-fold upon visible ($\lambda > 420$ nm) irradiation (b) as shown in Figures 1 and 2. This suggests that a primary product of the reaction between laser-ablated molybdenum atoms and CH_3Cl is responsible for the II absorptions, which is later converted to another product upon visible photolysis, resulting in an increase of the III absorptions. There appear to be two matrix environmental effects on the III bands as the 1828.5 cm^{-1} peak is produced on vis irradiation, while the 1836.8 cm^{-1} peak is favored on annealing.

Figure 2 shows the IR spectra in the regions 1400−1250 and 760−500 cm^{-1} for laser-ablated Mo atoms codeposited with

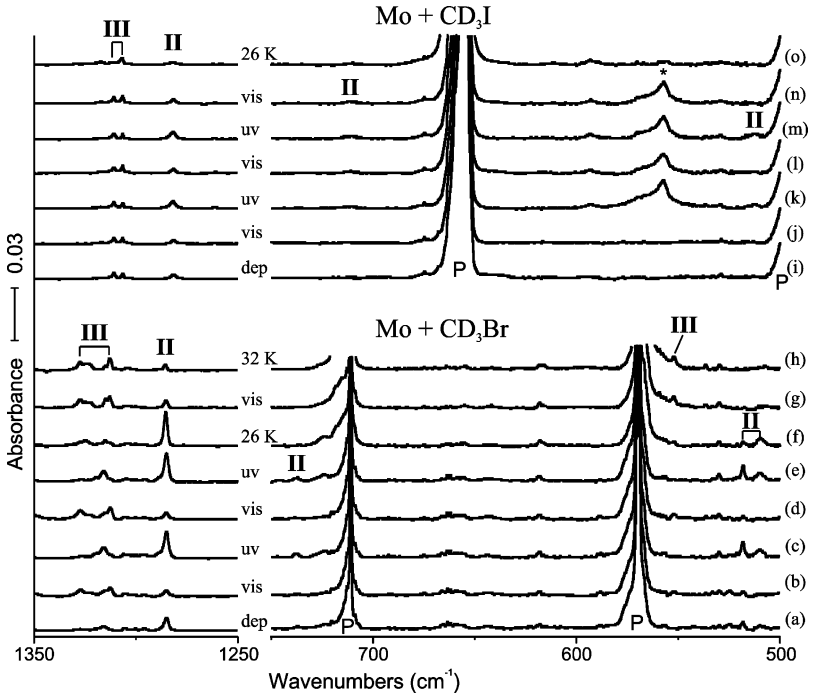

Figure 4. Infrared spectra in the regions of 1400−1250 and 750−500 cm^{-1} for laser-ablated Mo atoms codeposited with CD_3Br and CD_3I in excess argon at 8 K and their variations. (a) Mo + 0.5% CD_3Br in Ar codeposited for 1 h. (b) After broadband photolysis with a filter (λ > 420 nm) for 15 min. (c) After broadband photolysis with a filter (240 < λ < 380 nm) for 15 min. (d) After broadband photolysis with a filter (λ > 420 nm) for 15 min. (e) After broadband photolysis with a filter (240 < λ < 380 nm) for 15 min. (f) After annealing to 26 K. (g) After broadband photolysis with a filter (λ > 420 nm) for 15 min. (h) After annealing to 32 K. (i) Mo + 1.0% CD_3I in Ar codeposited for 1 h. (j) After broadband photolysis with a filter (λ > 420 nm) for 20 min. (k) After broadband photolysis with a filter (240 < λ < 380 nm) for 20 min. (l) After broadband photolysis with a filter (λ > 420 nm) for 20 min. (m) After broadband photolysis with a filter (240 < λ < 380 nm) for 20 min. (n) After broadband photolysis with a filter (λ > 420 nm) for 20 min. (o) After annealing to 26 K. II and III stand for the product absorption groups. P and * denote precursor and unidentified absorptions.

Ar/CD_3Cl (a) and their variation upon photolysis and annealing (b−h). The same photoreversibility is observed: the II absorptions decrease and increase upon visible and UV irradiation, respectively, while the III absorptions increase and decrease instead. The observed product absorptions are assigned on the basis of variation of vibrational characteristics upon isotopic substitution, frequency calculations, and comparison to previous results for similar small transition-metal complexes.[6] We will show below that CH_2═MoHCl and CH≡MoH_2Cl, the double- and triple-bonded insertion complexes, are responsible for the II and III absorptions, respectively.

Among the absorptions marked II in Figure 1, the absorption at 1789.5 cm^{-1} is most distinctive, appearing in a relatively clean area. It shows a large deuterium shift of −503.0 cm^{-1} (H/D ratio of 1.391), indicating that it is a hydrogen stretching absorption. The observed frequencies are also close to the hydrogen stretching frequencies of 1812.1 and 1761.9 cm^{-1} for MoH_4 and 1301.9 and 1265.5 cm^{-1} for MoD_4,[27] which are not found in this study. The observed Mo−H stretching frequencies are also near those of CH_2═MoHF as listed in Table 1. Clearly, a Mo−H bond is formed in the reaction of a Mo atom with CH_3Cl. Previous studies show that C−X insertion takes place first in the reaction of metal atoms with methyl halides, and the excess reaction energy leads to α-hydrogen transfer, resulting in formation of the methylidene complex (CH_2═MHX).[4−6]

However, absorptions from the first insertion complexes (CH_3−MoX) with heavy halogens (Cl, Br, and I) are not observed in this study, while those from higher oxidation-state complexes are clearly observed as shown in Figures 1−6. On the other hand, the single-, double-, and triple-bonded insertion complexes (CH_3−MoF, CH_2═MoHF, and CH≡MoH_2F) are all identified in previous studies of Mo + CH_3F.[6] Calculated harmonic vibrational modes for the methyl, methylidene, and methylidyne Mo complexes (CH_3−MoX, CH_2═MoHX and CH≡MoH_2X) using the hybrid density functional B3LYP and 6-311++G(3df,3pd)/SDD basis sets are listed in Tables 2−4. Pure density functional BPW91 calculations also give very similar results (Table 5). We show in Table 2 that, unlike the case of CH_3−MoF, the C−Mo and Mo−X stretching frequencies of methyl−metal complexes with heavy halogen ligands are quite low and out of our observation range, and the other bands are predicted to be considerably weak.

The II absorption at 847.7 cm^{-1} (not shown) gives a D isotopic shift of −105.2 cm^{-1} (H/D ratios of 1.142), and on the basis of the frequency and previous results for Mo + CH_3F, it is attributed to the predominantly C═Mo stretching mode, which is also mixed with hydrogen motion. The II absorption at 659.4 cm^{-1} has its deuterium counterpart at 515.5 cm^{-1} (H/D ratio of 1.279) and is assigned to the CH_2 out-of-plane wagging mode. The observed vibrational characteristics of the II absorptions indicate formation of the methylidene complex and are also in good agreement with the three most intense calculated harmonic frequencies listed in Table 3. The harmonic B3LYP calculation predicts the strong Mo−H stretch and CH_2 wag about 5% high as expected,[6,27,28] and the anharmonic calculation approaches the experimental values and comes in about 1% too high. The mixed C═Mo stretching mode is the most difficult to model, and the harmonic computation splits the two matrix site bands, but the anharmonic value is 21 cm^{-1} too low in this case. The II frequencies are consistent as well with those of previously studied groups 4, 5, and 6 metal methylidene complexes,[4−10] affirming formation of the methylidene complex (CH_2═MoHCl).

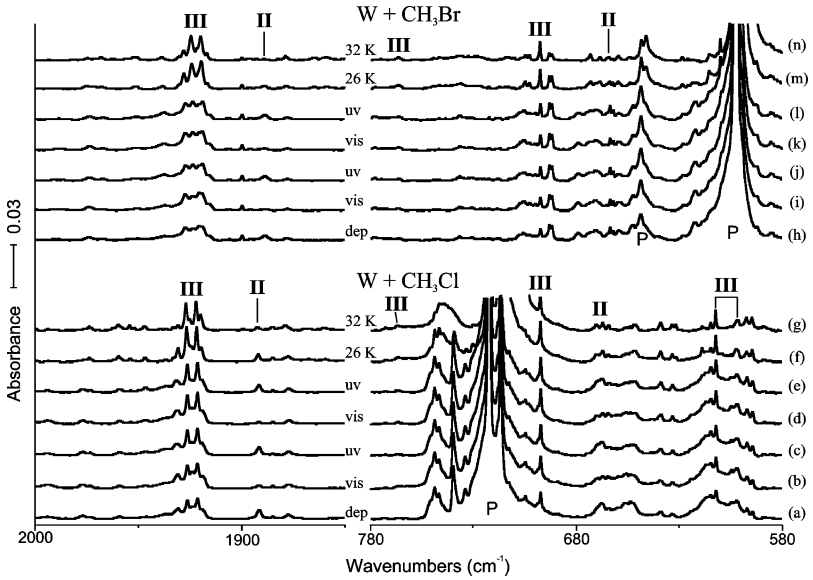

Figure 5. Infrared spectra in the regions 2000−1850 and 780−580 cm^{-1} for laser-ablated W atoms codeposited with CH_3Cl and CH_3Br in excess argon at 8 K and their variations. (a) W + 0.5% CH_3Cl in Ar codeposited for 1 h. (b) After broadband photolysis with a filter (λ > 420 nm) for 15 min. (c) After broadband photolysis with a filter (240 < λ < 380 nm) for 15 min. (d) After broadband photolysis with a filter (λ > 420 nm) for 30 min. (e) After broadband photolysis with a filter (240 < λ < 380 nm) for 15 min. (f) After annealing to 26 K. (g) After annealing to 32 K. (h) W + 0.5% CH_3Br in Ar codeposited for 1 h. (i) After broadband photolysis with a filter (λ > 420 nm) for 15 min. (j) After broadband photolysis with a filter (240 < λ < 380 nm) for 15 min. (k) After broadband photolysis with a filter (λ > 420 nm) for 15 min. (l) After broadband photolysis with a filter (240 < λ < 380 nm) for 15 min. (m) After annealing to 26 K. (n) After annealing to 32 K. II and III denote the product absorption groups and P indicates precursor absorption.

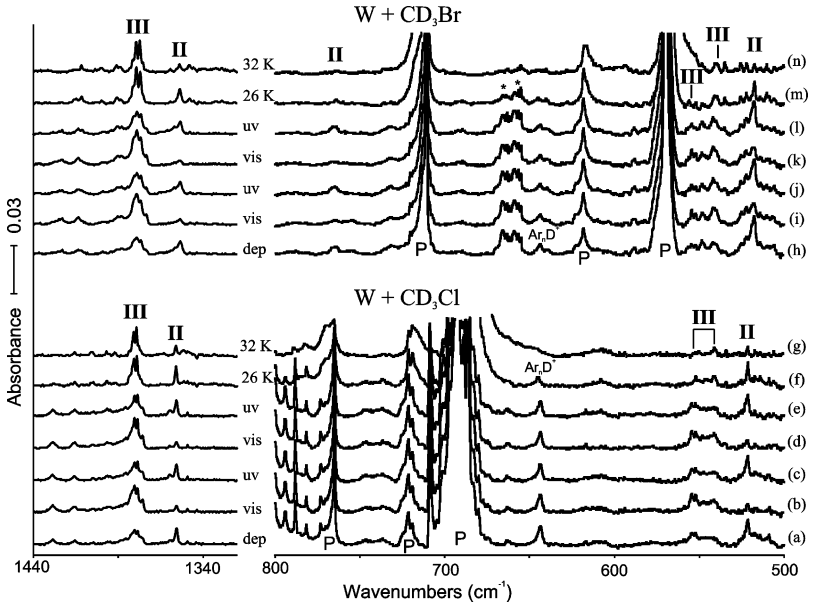

Figure 6. Infrared spectra in the regions 1440−1320 and 800−500 cm^{-1} for laser-ablated W atoms codeposited with CD_3Cl and CD_3Br in excess argon at 8 K and their variations. (a) W + 0.5% CD_3Cl in Ar codeposited for 1 h. (b) After broadband photolysis with a filter (λ > 420 nm) for 15 min. (c) After broadband photolysis with a filter (240 < λ < 380 nm) for 15 min. (d) After broadband photolysis with a filter (λ > 420 nm) for 30 min. (e) After broadband photolysis with a filter (240 < λ < 380 nm) for 15 min. (f) After annealing to 26 K. (g) After annealing to 32 K. (h) W + 0.5% CD_3Br in Ar codeposited for 1 h. (i) After broadband photolysis with a filter (λ > 420 nm) for 15 min. (j) After broadband photolysis with a filter (240 < λ < 380 nm) for 15 min. (k) After broadband photolysis with a filter (λ > 420 nm) for 15 min. (l) After broadband photolysis with a filter (240 < λ < 380 nm) for 15 min. (m) After annealing to 26 K. (n) After annealing to 32 K. II and III stand for the product absorption groups. P and * denote precursor and unidentified absorptions.

The III absorptions at 1840.7 and 1836.8 cm^{-1} have their deuterium counterparts at 1325.8 and 1315.7 cm^{-1} (H/D ratios of 1.388 and 1.396), respectively, which is characteristic of Mo−H stretching absorptions. Although the harmonic calculations predict the stronger antisymmetric stretching mode higher by 3 cm^{-1} than the weaker symmertric mode, the anharmonic calculations reverse this order and find a 1 cm^{-1} separation. The stronger, lower band may in fact be due to the antisymmetric mode, but we cannot be certain in this close-run situation. In any case, previous studies show that the higher oxidation state of Mo leads to higher hydrogen stretching frequencies,[6,9,27] suggesting that the III absorptions arise from a higher oxidation-state complex than CH_2═MoHCl with strong Mo−H absorption at 1789.5 cm^{-1}. The frequencies are in fact close to those of CH≡MoH_2F (1844.8 cm^{-1}) and CH≡MoH_3 (1830.0 cm^{-1}) and may be compared with the hydrogen stretching absorption of

TABLE 2: Calculated Harmonic Fundamental Frequencies of CH_3-MoX Isotopomers in the Ground $^4A''$ Electronic State[a]

	CH_3-MoF		CD_3-MoF		$^{13}CH_3-MoF$		CH_3-MoCl		CD_3-MoCl		CH_3-MoBr		CD_3-MoBr		CH_3-MoI		CD_3-MoI	
description	freq	int	freq	int	freq	int	freq	int	freq	int	freq	int	freq	int	freq	int	freq	int
A′ CH_3 str.	3051.3	9	2240.5	4	3042.5	9	3053.4	9	2239.4	5	3053.0	8	2239.5	5	3054.0	8	2239.7	5
A′ CH_3 str.	2931.0	11	2111.4	3	2925.8	11	2916.5	15	2103.0	5	2918.0	16	2103.6	5	2915.4	15	2101.9	5
A′ CH_3 bend	1440.6	2	1046.7	2	1437.2	2	1439.4	3	1046.1	2	1438.6	2	1045.6	2	1437.8	3	1045.2	2
A′ CH_3 deform	1186.4	5	927.7	4	1177.3	5	1184.6	4	925.8	1	1183.6	3	925.1	1	1183.9	4	925.4	1
A′ CH_3 rock	594.3	15	504.7	20	584.9	13	587.7	10	501.5	19	583.4	9	498.7	18	582.0	8	498.9	19
A′ C−Mo str.	448.6	23	371.5	11	440.0	23	444.3	52	387.6	67	442.0	45	361.4	29	440.0	46	356.5	27
A′ Mo-X str.	628.8	148	628.6	146	628.8	148	372.6	42	348.0	9	264.3	25	261.5	22	207.1	17	205.2	16
A′ CMoX bend	119.5	5	107.5	5	118.3	5	98.8	2	89.6	2	87.1	1	78.2	1	80.5	1	71.8	1
A″ CH_3 str.	3094.1	3	2290.7	1	3082.9	3	3098.7	2	2294.3	0	3098.2	2	2293.9	0	3099.8	2	2295.1	0
A″ CH_3 bend	1400.2	2	1016.9	2	1397.0	1	1394.4	2	1013.3	2	1394.5	3	1013.5	2	1392.5	2	1012.3	2
A″ CH_3 rock	588.2	15	438.1	9	585.3	15	577.9	14	429.9	9	575.4	14	427.8	8	570.6	15	424.1	9
A″ CH_3 distort	153.8	0	111.7	0	153.7	0	132.7	0	96.2	0	121.8	0	87.9	0	109.9	0	79.2	0

[a] Frequencies and intensities are in cm^{-1} and km/mol, respectively. Calculated using B3LYP and 6-311++G(3df,3pd)/SDD basis set. ^{35}Cl, ^{79}Br, and ^{98}Mo are assumed in calculations.

TABLE 3: Calculated Harmonic Fundamental Frequencies of $CH_2=MoHX$ Isotopomers in the Ground ^2A Electronic State[a]

	$CH_2=MoHF$		$CD_2=MoDF$		$^{13}CH_2=MoHF$		$CH_2=MoHCl$		$CD_2=MoDCl$		$CH_2=MoHBr$		$CD_2=MoDBr$		$CH_2=MoHI$		$CD_2=MoDI$	
description	freq	int	freq	int	freq	int	freq	int	freq	int	freq	int	freq	int	freq	int	freq	int
A′ C−H str.	3227.4	7	2392.4	7	3216.2	7	3222.5	7	2388.4	7	3220.0	7	2386.5	7	3219.0	8	2385.7	8
A′ C−H str.	2775.7	5	2019.1	4	2769.4	5	2750.0	8	2000.1	6	2753.8	9	2002.6	6	2735.1	12	1988.9	8
A′ Mo−H str.	1893.0	170	1346.4	88	1892.9	170	1881.3	156	1338.1	82	1878.3	166	1335.9	85	1887.1	166	1342.1	85
A′ CH_2 scis.	1356.8	23	1064.5	17	1347.7	24	1350.4	22	1057.5	17	1344.1	21	1054.3	18	1345.0	21	1054.0	18
A′ C=Mo str.	835.4	72	730.5	48	818.9	86	837.4	64	731.5	40	833.8	62	727.5	40	838.9	64	732.9	44
A′ CMoH bend	803.4	21	587.4	13	795.9	8	802.8	1	616.0	11	798.6	0	610.7	7	802.0	0	613.0	5
A′ CH_2 rock	503.2	13	383.3	6	500.0	12	489.7	2	388.1	36	472.7	4	350.7	1	479.8	8	353.0	3
A′ Mo−X str.	634.5	113	655.9	128	633.9	111	382.0	58	354.2	19	271.9	29	268.0	28	214.9	19	211.5	19
A′ CMoX bend	191.9	2	174.3	2	190.3	2	144.4	2	130.4	1	127.2	2	114.2	1	118.1	2	105.9	2
A″ CH_2 wag	680.1	73	530.8	49	674.6	71	692.8	71	539.4	46	687.3	70	534.6	46	688.1	72	535.2	47
A″ CH_2 twist	455.9	17	331.8	6	455.8	17	406.8	16	291.9	7	391.4	17	279.4	8	370.3	17	263.8	8
A″ MoH oop bend	107.3	45	82.0	26	107.0	45	107.9	38	84.4	21	120.6	35	90.3	19	178.1	32	129.1	17

[a] Frequencies and intensities are in cm^{-1} and km/mol, respectively. Calculated using B3LYP and 6-311++G(3df,3pd)/SDD basis set. ^{35}Cl, ^{79}Br, and ^{98}Mo are assumed in calculations.

TABLE 4: Calculated Harmonic Fundamental Frequencies of $CH\equiv MoH_2X$ Isotopomers in the Ground $^1A_1$ Electronic State[a]

	$CH\equiv MoH_2F$		$CD\equiv MoD_2F$		$^{13}CH\equiv MoH_2F$		$CH\equiv MoH_2Cl$		$CD\equiv MoD_2Cl$		$CH\equiv MoH_2Br$		$CD\equiv MoD_2Br$		$CH\equiv MoH_2I$		$CD\equiv MoD_2I$	
description	freq	int	freq	int	freq	int	freq	int.	freq	int	freq	int	freq	int	freq	int	freq	int
A′ C−H str.	3201.2	16	2379.6	14	3189.5	16	3209.4	15	2385.6	13	3207.3	15	2384.0	13	3206.1	16	2383.4	14
A′ MoH_2 str.	1944.9	132	1379.9	70	1944.9	132	1933.1	156	1371.3	82	1931.6	171	1370.3	90	1935.8	185	1373.3	98
A′ C≡Mo str.	1052.5	16	1005.9	13	1019.9	15	1050.2	13	1003.7	12	1045.0	13	1003.4	12	1052.0	14	1005.3	12
A′ MoH_2 scis.	794.3	100	679.2	140	794.3	101	799.9	43	586.3	15	795.9	34	587.6	14	787.8	28	583.5	12
A′ MoH_2 wag	726.9	42	567.5	3	722.1	42	741.9	42	575.1	48	743.1	44	567.4	37	736.8	45	558.3	35
A′ MoCH bend	563.9	113	415.2	47	562.8	113	600.6	59	440.7	16	602.3	65	434.6	28	593.4	68	427.0	30
A′ Mo-X str.	646.5	25	535.1	15	645.7	24	390.9	50	376.4	50	280.2	24	274.4	24	220.8	17	215.9	16
A′ CMoX bend	260.5	5	241.5	6	265.9	5	207.4	2	190.9	2	184.8	2	169.6	1	162.5	2	149.5	1
A″ MoH_2 str.	1945.5	215	1388.5	112	1945.5	215	1936.6	179	1382.2	92	1935.8	172	1381.7	89	1940.5	159	1384.9	82
A″ CH oop bend	823.4	0	654.7	1	815.4	0	836.0	1	664.6	1	835.4	1	663.5	1	833.4	1	661.9	1
A″ MoH_2 deform.	584.9	84	417.1	44	584.7	84	589.0	66	417.5	33	589.9	63	418.0	32	582.5	66	412.9	33
A″ MoH_2 rock	423.4	0	317.8	0	423.2	0	364.9	0	268.7	0	342.8	0	250.1	0	300.0	0	217.4	0

[a] Frequencies and intensities are in cm^{-1} and km/mol, respectively. Calculated using B3LYP and 6-311++G(3df,3pd)/SDD basis set. ^{35}Cl, ^{79}Br, and ^{98}Mo are assumed in calculations.

MoH_6 at 1857.6 cm^{-1}.[27] However, the absorptions of binary Mo hydrides are not observed here. Therefore, the photoreversibility between the II and III absorptions arises from interconversion between the methylidene and methylidyne complexes ($CH_2=MoHCl$ and $CH\equiv MoH_2Cl$) via α-hydrogen migration, as presented in Scheme 1. Our DFT calculations find the methylidyne complex 4 kcal/mol higher in energy than the methylidene complex. (See Tables S1, S2, and S3 for computed energies.)

The vibrational characteristics of other III absorptions also support the formation of $CH\equiv MoH_2Cl$. The absorption at 765.8 cm^{-1} shows a D isotopic shift of −197.6 cm^{-1} (H/D ratio of 1.348) and is attributed to the MoH_2 bending mode. The MoH_2 wagging absorption is overlapped by the strong precursor C−Cl stretching absorption, but the deuterium counterpart is observed at 561.0 cm^{-1}. The deuterium counterparts of the III absorptions at 572.8 and 568.2 cm^{-1} are not observed due to their low frequencies. The latter bands are assigned to the A′ MoCH bending and A″ MoH_2 deformation modes. The observed vibrational characteristics are in very good agreement with the calculated harmonic values for $CH\equiv MoH_2Cl$ (listed in Table 4) considering the approximations involved.

Notice in Table 5 that the calculated harmonic values using the B3LYP functional are all higher as expected,[28,29] ranging from about 4% to 5% depending on the normal mode. The harmonic frequencies using the BPW91 functional are 2% to 3% higher with the exception of the MoH_2 bending mode, which is not as well-described by the pure density functional. Scale

TABLE 5: Comparison of Observed (Argon Matrix) and Calculated (DFT) Harmonic and Anharmonic Frequencies for the CH≡MoH_2Cl and CH≡MoH_2Br Complexes[a]

CH≡MoH_2Cl				CH≡MoH_2Br				
observed	harm B3LYP	harm BPW91	anharm B3LYP	observed	harm B3LYP	harm BPW91	anharm B3LYP	mode descript
1840.7	1936.1(0.951)[b]	1904.7(0.966)[b]	1860.0(0.990)[b]	1843.7	1935.8(0.952)[b]	1901.8(0.969)[b]	1856.9(0.993)[b]	A″ MoH_2 str.
1835.8	1932.6(0.950)	1898.5(0.967)	1861.3(0.986)	1831.2	1931.6(0.948)	1895.1(0.966)	1858.1(0.986)	A′ MoH_2 str.
765.8	800.1(0.957)	824.7(0.924)	765.4(1.001)	752.3	795.9(0.945)	817.1(0.921)	777.8(0.967)	A′ MoH_2 bend.
c	741.9	719.2	716.3	714.9	743.1(0.962)	719.8(0.993)	713.7(1.002)	A′ MoH_2 wag
572.8	600.7(0.954)	588.3(0.974)	591.7(0.968)	569.0	602.3(0.945)	586.9(0.970)	576.3(0.987)	A′ MoCH bend
568.2	589.0(0.965)	579.7(0.980)	574.5(0.989)	562.4	589.8(0.954)	579.5(0.970)	559.5(1.005)	A″ MoH_2 def

[a] All calculations used 6-311++G(3df,3pd)/SDD basis set, and all frequencies are in cm^{-1}. Observed in an argon matrix. Description gives major coordinate. [b] Scale factors (observed/calculated frequencies). [c] Overlapped by precursor band.

SCHEME 1

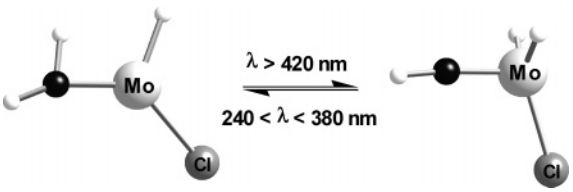

factors (observed/calculated frequencies) are also given in Table 5. Finally, anharmonic frequencies calculated using the B3LYP functional are much closer to the observed measurements with most values 1−2% higher than the observed frequencies. It could be argued that the matrix shift accounts for much of this difference. However, vibrational modes are not created equally, and the anharmonicities differ, which is shown by the variation in anharmonic scale factors in Table 5, particularly for the lower-frequency bending modes. Bending potential functions are clearly more difficult to define mathematically than stretching potential functions, and accordingly, the anharmonic corrections for these lower-frequency modes are more approximate than those for the higher-frequency stretching modes.

The overall reaction mechanism proceeds as given in reaction 1. The metal atom is excited in the laser-ablation process or by UV irradiation. These reactions do not proceed on annealing, as activation energy is required. Photochemical rearrangement between the methylidene and methylidyne complexes is shown in Scheme 1. A comparison of the reactivity of Zr, Nb, and Mo atoms with CH_3Cl based on the strong M−H stretching mode absorbance normalized by calculated intensity for the common CH_2═MHX products formed on UV irradiation (240−380 nm) in similar experiments finds Zr more reactive (band absorbance 0.05/calculated band intensity 400 km/mol)[4e] than Nb (band absorbance 0.01/ calculated band intensity 284 km/mol)[5b] but less reactive than Mo (band absorbance 0.04/ calculated band intensity 170 km/mol). The greater reactivity observed for Zr in these experiments is in contrast to the smaller number of zirconium alkylidene complexes in synthetic chemistry reviewed by Schrock as compared to niobium, but molybdenum is more reactive here, and more alkylidene complexes are found with this group 4 metal.[2a]

$$M^* + CH_3X \rightarrow CH_3{-}MX \rightarrow CH_2{=}MHX \leftrightarrow CH{\equiv}MH_2X \quad (1)$$

Mo + CH_3Br. The spectra observed from the Mo + CH_3Br reaction products shown in Figures 3 and 4 are similar to those from the Mo + CH_3Cl reaction. Two sets of absorptions are also observed on the basis of variations in intensity upon photolysis and annealing. The absorptions marked II are evident after deposition (a) but decrease more than 50% upon visible irradiation (b) and increase dramatically after UV irradiation, ending up doubled in total (c). The absorptions marked III are relatively weak after deposition (a) but triple following visible irradiation (b) and decrease upon UV irradiation (c). They sharpen and decrease in the process of annealing (f and h). Again, matrix effects are found with an 1825.1 cm^{-1} peak produced on vis irradiation and 1831.2 cm^{-1} band favored on annealing. Parallel to the Mo + CH_3F and Mo + CH_3Cl cases, the two sets of absorptions form a photoreversible system.

The strong II absorption at 1787.3 cm^{-1} along with its deuterium counterpart at 1284.9 (H/D ratio of 1.391) undoubtedly originate from the Mo−H and Mo−D stretching modes. This shows that C−X insertion by the Mo atom readily occurs regardless of halogen size, followed by α-hydrogen transfer to form CH_2═MoHBr. The II absorption at 845.7 cm^{-1} (not shown) and its deuterium counterpart at 737.7 cm^{-1} (H/D ratio of 1.146) are attributed to the mostly C═Mo stretching mode in line with the Mo + CH_3Cl case. The strong absorption at 654.5 cm^{-1} shows a D isotopic shift of −144.7 cm^{-1} (H/D ratio of 1.284) and is assigned to the CH_2 wagging mode on the basis of the frequency and isotopic shift. The Mo−Br stretching absorption is not observed due to its low frequency. Again, the computed harmonic frequencies are about 5% too high for the Mo−H and CH_2 modes (Table 3), and the anharmonic values are nearly 1% too high, but the mixed C═Mo mode is better approximated by the harmonic than the 30 cm^{-1} lower anharmonic prediction. The observed vibrational characteristics support formation of the methylidene complex (CH_2═MoHBr).

The III absorptions at 1843.7 and 1831.2 cm^{-1} have their deuterium counterparts at 1327.2 and 1312.5 cm^{-1} (H/D ratios of 1.389 and 1.395), respectively, and parallel to the Mo + CH_3-Cl case, they are attributed to the antisymmetric and symmetric MoH_2 stretching modes, respectively. The hydrogen stretching absorption pair on the blue side of the Mo−H stretching absorption of CH_2═MoHBr, along with consistent calculation results, suggests that a higher oxidation-state Mo complex (CH≡MoH_2Br) is also formed. This indicates that conversion of CH_2═MoHBr to CH≡MoH_2Br via α-hydrogen migration also readily occurs parallel to the Mo + CH_3F and Mo + CH_3Cl systems.

The III absorption at 752.3 cm^{-1} is attributed to the MoH_2 bending mode in line with the Mo + CH_3F and Mo + CH_3Cl cases, while the deuterium counterpart is believed to be overlapped by the strong C−Br stretching absorption of the precursor. The III band at 714.9 cm^{-1} shows a D shift of −162.7 cm^{-1} (H/D ratio of 1.294) and is assigned to the MoH_2 wagging mode on the basis of the calculation and consistency with the previous cases. On the further lower-frequency side, two more III absorptions are observed at 569.0 and 562.4 cm^{-1}, and they are assigned to the A′ MoCH bending and A″ MoH_2 deformation modes, while the deuterium counterparts are not observed due to their low frequencies. The observed vibrational characteristics are in the range of agreement expected with the harmonic calculated values for CH≡MoH_2Br in Table 4, and

TABLE 6: Frequencies of Product Absorptions Observed from Reactions of Methyl Halides with W Atoms in Excess Argon[a]

group	CH_3F	CD_3F	$^{13}CH_3F$	CH_3Cl	CD_3Cl	CH_3Br	CD_3Br	description
II	1905.6	1365.6	1905.6	1891.5	1355.8	1888.8	1353.5	A′ W−H str.
		758.3		853.7	*b*	853.4	765.2	A′ C═W str,
	683.4	525.3	678.4	667.5	521.5	663.6	517.5	A″ CH_2 wag
	651.2	656.8	648.4					A′ W−X str.
III	1936.4	1386.4	1936.3	1926.2	1380.4	1924.1	1379.5	A′ WH_2 str.
	1930.4	1386.4	1930.3	1921.4	1378.6	1919.5	1377.4	A" WH_2 str.
	780.4	682.3	780.2	766.8	554.5	766.4	554.4	A′ WH_2 scis.
	705.1	532.6	701.7	697.2	540.8	697.4	539.9	A′ WH_2 wag
	589.3		588.4	612.2		*b*		A′ WCH bend
	605.0		605.0	602.0		*b*		A″ WH_2 deform

[a] All frequencies are in cm^{-1}. Description gives major coordinate. [b] Overlapped by precursor band.

TABLE 7: Calculated Harmonic Fundamental Frequencies of CH_3-WX Isotopomers in the Ground $^4A''$ Electronic State[a]

	CH_3-WF		CD_3-WF		$^{13}CH_3-WF$		CH_3-WCl		CD_3-WCl		CH_3-WBr		CD_3-WBr	
description	freq	int	freq	int	freq	int	freq	int	freq	int	freq	int	freq	int
A′ CH_3 str.	3040.5	12	2227.4	6	3033.3	12	3042.6	10	2227.6	5	3042.0	10	2226.8	5
A′ CH_3 str.	2902.6	8	2095.6	3	2897.0	9	2896.0	9	2091.8	3	2893.3	9	2090.0	3
A′ CH_3 bend	1441.9	5	1047.8	3	1438.6	4	1438.4	5	1045.5	3	1437.2	5	1044.7	3
A′ CH_3 deform	1206.2	6	943.3	6	1197.0	0	1204.2	3	942.1	5	1202.5	3	941.0	5
A′ CH_3 rock	607.8	42	522.8	13	598.2	23	604.7	7	517.3	11	601.7	8	515.2	13
A′ C−W str.	433.5	21	355.4	11	425.7	21	424.1	39	371.6	57	419.3	36	339.5	23
A′ W−X str.	631.4	93	626.8	126	629.4	111	366.3	39	338.4	7	246.3	19	245.0	18
A′ CWX bend	116.0	1	102.4	2	114.4	2	99.8	1	90.0	1	88.6	0	78.7	0
A″ CH_3 str.	3083.2	3	2282.5	1	3072.0	4	3087.4	2	2285.6	1	3087.7	2	2286.0	1
A″ CH_3 bend	1389.6	1	1008.3	1	1386.5	2	1386.3	2	1006.3	1	1385.0	2	1005.4	1
A″ CH_3 rock	614.8	9	458.5	5	611.8	9	606.2	9	451.8	5	602.5	9	449.0	5
A″ CH_3 distort	190.1	0	139.3	0	190.0	0	165.0	1	119.8	0	158.6	1	114.1	0

[a] Frequencies and intensities are in cm^{-1} and km/mol. Calculated using B3LYP and 6-311++G(3df,3pd)/SDD basis set. ^{35}Cl, ^{79}Br, and ^{184}W are assumed in calculations..

the BPW91 values (Table 5) are closer (higher scale factors) than the B3LYP values (lower scale factors) to the observed values. Again, the anharmonic frequencies are still closer to the observed values, and the scale factors are higher. However, notice that the anharmonic scale factors for the MoH_2 bending mode, the Mo−C−H bending mode, and the MoH_2 rocking modes differ by 2% to 3% between the Cl and Br derivatives. The anharmonic calculation apparently incorporates more MoH_2 bending interaction with the halogen than the molecule requires. This underscores the difficulty in calculating accurate anharmonic potential functions, particularly for lower-frequency bending modes where nearby vibrational modes interact more strongly.

Mo + CH_3I. The spectra observed from the Mo + CH_3I reaction products are also shown in Figures 3 and 4. Previous attempts for reaction of CH_3I with laser-ablated metal atoms normally resulted in very weak product absorptions, probably due to rapid dissociation of the precursor by UV emission from the ablation plume.[30] To compensate the amount of dissociation during deposition, a relatively high concentration of 1.0% CH_3I in argon is used in this study. The photoreversible II absorptions are evident in Figure 3, but the III hydrogen stretching absorptions are only barely discernible on the blue side of the II absorptions at 1783.7 cm^{-1}.

The II absorption at 1783.7 cm^{-1} is almost undoubtedly the Mo−H stretching band of CH_2═MoHI in line with the previous Mo + CH_3X cases. The weak absorption at 820.7 cm^{-1} and its deuterium counterpart at 711.4 cm^{-1} (H/D ratio of 1.154) are assigned to the C═Mo stretching mode, and the absorption at 649.5 cm^{-1} with its deuterium counterpart at 512.2 cm^{-1} (H/D ratio of 1.268) are designated to the CH_2 wagging mode on the basis of the frequency and isotopic shift. The observed absorptions correspond to the strongest bands of the methylidene complex, CH_2═MoHI, and the vibrational characteristics are in good agreement with the calculated values shown in Table 3.

The III absorptions are very weak. The bands at 1845.5 and 1825.1 cm^{-1} are assigned to the antisymmetric and symmetric MoH_2 stretching modes of the methylidyne complex (CH≡MoH_2I), which are consistent with the previous Mo + CH_3X cases. The absorptions at 1317.1 and 1306.5 cm^{-1} with Mo + CD_3I (H/D ratios of 1.401 and 1.397) are relatively sharper and show less changes in intensity upon photolysis, and are assigned to the MoD_2 stretching modes. The much weaker III absorptions relative to the II absorptions in the Mo + CH_3I spectra suggest that the methylidyne complexes become less favored with increasing halogen size. As a matter of fact, the intensities of the methylidyne absorptions relative to those of the methylidene absorptions are highest in the Mo + CH_3F spectra. These results suggest that, in the Mo system, the triple-bonded product is relatively less favored with increasing halogen size.

W + CH_3Cl. Shown in Figure 5 are the infrared spectra in the regions of 2000−1850 and 780−580 cm^{-1} observed from the products of W reactions with CH_3Cl and CH_3Br, and the frequencies are listed in Table 6. Parallel to the Mo systems, the II and III absorptions arise from the methylidene and methylidyne complexes (CH_2═WHCl and CH≡WH_2Cl). Clearly, the III absorptions are relatively much stronger than the II absorptions in comparison with the Mo + CH_3X systems. This is consistent with previous results that high-oxidation-state complexes are more favored with heavier metals in the same group of early transition metals.[4−10]

Parallel to the Mo cases above, the II absorptions decrease and increase upon visible and UV irradiation, respectively. Increases in intensity of II absorptions are accompanied with decreases in intensity of III absorptions, and vice versa. They, as a result, form photoreversible pairs, which are more evident in the spectra of deuterated precursors shown in Figure 6. The methylidyne complexes are produced less in reactions of the deuterated precursors as shown in Figures 5 and 6, due to less efficient α-deuterium migration. Because of the lower original

TABLE 8: Calculated Harmonic Fundamental Frequencies of CH_2═WHX Isotopomers in the Ground ^2A Electronic State[a]

	CH_2═WHF		CD_2═WDF		$^{13}CH_2$═WHF		CH_2═WHCl		CD_2═WDCl		CH_2═WHBr		CD_2═WDBr	
description	freq	int	freq	int	freq	int	freq	int	freq	int	freq	int	freq	int
A′ C−H str.	3248.9	7	2409.0	8	3237.5	7	3242.8	8	2404.0	9	3239.5	8	2401.5	9
A′ C−H str.	2750.7	6	2002.3	5	2744.4	6	2724.1	10	1982.6	7	2723.1	12	1981.6	8
A′ W−H str.	1969.2	112	1397.2	57	1969.2	112	1961.0	119	1391.2	60	1957.8	124	1388.9	63
A′ CH_2 scis.	1368.6	22	1069.8	15	1359.9	22	1362.7	22	1065.2	18	1357.2	21	1062.5	19
A′ C═W str.	860.6	41	751.3	26	838.1	43	857.1	44	749.2	30	854.8	46	746.5	32
A′ CWH bend	790.6	28	581.1	5	786.8	25	783.8	8	592.1	10	780.2	6	587.7	6
A′ CH_2 rock	533.8	20	405.7	6	530.4	19	525.5	5	399.4	5	510.7	10	379.9	3
A′ W−X str.	644.4	100	656.4	133	643.9	100	373.6	55	363.8	48	252.8	24	251.0	25
A′ CWX bend	182.4	1	165.3	1	180.3	1	142.0	1	128.0	1	125.6	1	112.2	1
A″ CH_2 wag	714.6	73	556.9	38	708.9	57	703.8	61	547.7	39	698.0	61	543.0	39
A″ CH_2 twist	420.8	14	307.2	6	420.8	14	373.0	15	267.9	7	352.3	15	251.6	7
A″ WH oop bend	95.1	27	71.1	15	94.9	28	122.9	24	92.3	13	137.0	23	100.6	12

[a] Frequencies and intensities are in cm^{-1} and km/mol. Calculated using B3LYP and 6-311++G(3df,3pd)/SDD basis set. ^{35}Cl, ^{79}Br, and ^{184}W are assumed in calculations..

TABLE 9: Calculated Harmonic Fundamental Frequencies of CH≡WH_2X Isotopomers in the Ground $^1A_1$ Electronic State[a]

	CH≡WH_2F		CD≡WD_2F		^{13}CH≡WH_2F		CH≡WH_2Cl		CD≡WD_2Cl		CH≡WH_2Br		CD≡WD_2Br	
description	freq	int	freq	int	freq	int	freq	int	freq	int	freq	int	freq	int
A′ C−H str.	3235.0	15	2405.9	13	3224.0	15	3236.6	16	2406.7	13	3234.0	16	2404.8	13
A′ WH_2 str.	2001.2	117	1418.1	60	2001.2	117	1996.0	143	1414.4	74	1994.6	156	1413.4	81
A′ C≡W str.	1050.7	12	1002.0	10	1016.0	12	1049.3	12	1000.4	11	1048.9	13	999.9	11
A′ WH_2 scis.	806.2	67	676.7	112	806.0	69	788.5	25	577.5	5	786.8	18	579.6	11
A′ WH_2 wag	726.8	52	571.9	13	722.3	49	728.1	51	555.9	53	728.1	60	550.0	42
A′ WCH bend	606.4	103	452.5	34	605.8	606	639.2	58	463.2	18	634.9	57	455.4	23
A′ W−X str.	669.0	22	541.5	22	668.0	21	378.4	46	370.2	42	257.1	22	254.2	21
A′ CWX bend	253.4	4	237.7	4	249.5	4	198.5	1	183.5	1	177.9	1	163.5	1
A″ WH_2 str.	1994.4	178	1417.7	92	1994.4	178	1990.0	156	1414.4	80	1989.1	149	1413.7	76
A″ CH oop bend	801.7	8	635.8	7	794.0	7	800.8	6	634.5	5	799.3	6	633.4	5
A″ WH_2 deform.	627.8	71	446.1	36	627.8	71	620.7	63	439.8	31	616.3	60	436.3	30
A″ WH_2 rock	419.1	0	313.1	0	418.9	0	362.4	1	265.2	0	348.6	0	252.0	0

[a] Frequencies and intensities are in cm^{-1} and km/mol. Calculated using B3LYP and 6-311++G(3df,3pd)/SDD basis set. ^{35}Cl, ^{79}Br, and ^{184}W are assumed in calculations.

concentrations of the deuterated methylidyne complexes, the relative variations in absorption intensity upon photolysis are larger as shown in Figure 6. The II absorption at 1891.5 cm^{-1} and its deuterium counterpart at 1355.8 cm^{-1} (H/D ratio of 1.395) in the W + CH_3Cl spectra shown in Figures 5 and 6 are due to W−H and W−D stretching absorptions. The higher hydrogen stretching frequencies of the W products than those of the Mo products are attributable to larger relativistic contraction for the third-row transition metal as predicted by Pyykko et al.[31] The frequencies are compared with W−H stretching frequencies of 1911 and 1866.2 cm^{-1} for WH_4 and 1377.7 cm^{-1} for WD_4 in an argon matrix,[32] which are not observed in this study. They are also compared with the W−H stretching frequencies of 1905.6 and 1365.6 cm^{-1} of CH_2═WHF and CD_2═WDF (Table 6). The observed W−H stretching absorptions follow the reaction of W atoms with CH_3Cl, forming the CH_3−WCl intermediate, and then the methylidene complex, CH_2═WHCl, which is trapped in the matrix. The CH_3−WCl intermediate is not observed here, but calculated frequencies that support this conclusion are given in Table 7. The weak absorption at 853.7 cm^{-1} is attributed to the C═W stretching mode on the basis of the frequency, while the deuterium counterpart is overlapped by a precursor absorption. Another II absorption at 667.5 cm^{-1} with deuterium counterpart at 521.5 cm^{-1} (H/D ratio of 1.280) is due to the CH_2 wagging mode. The observed vibrational characteristics are in expected agreement with the harmonic calculated values for CH_2═WHCl listed in Table 8. We note similar agreement for the harmonic frequencies, and the anharmonic predictions are 1% low for the W−H mode, 1% high for the CH_2 mode and 18 cm^{-1} too low for the mixed C═W stretching mode.

Like the Mo systems described above, the intermediate insertion complex (CH_3−WX) is not identified in the spectra in Figures 5 and 6. Table 7 shows that the C−W and W−Cl stretching bands with highest absorption intensities are expected in too low of a frequency region to observe, and the other bands are all very weak. Moreover, the single insertion complexes are much less favored in heavy metal systems as described above. The III absorptions at 1924.1 and 1919.5 cm^{-1} in the W + CH_3Cl spectra have their deuterium counterparts at 1379.5 and 1377.4 cm^{-1} (H/D ratios of 1.395 and 1.394). The frequencies, which are ∼30 cm^{-1} higher than the W−H stretching frequencies of CH_2═WHCl, are compared with the hydrogen stretching frequency[32] at 1923.7 cm^{-1} for WH_6, which is not observed in this study. They are also compared with the antisymmetric and symmetric stretching frequencies of 1936.4 and 1930.4 cm^{-1} for CH≡WH_2F. They indicate that the methylidyne complex (CH≡WH_2Cl) is produced as a primary product in reaction of W with CH_3Cl.

The III absorption at 766.8 cm^{-1} shows a D isotopic shift of −212.3 cm^{-1} (H/D ratio of 1.383) and is assigned to the WH_2 bending mode. The absorption at 697.2 cm^{-1} has its deuterium counterpart at 540.8 cm^{-1} (H/D ratio of 1.289) and is attributed to the WH_2 wagging mode. The III absorptions at 612.2 and 602.0 cm^{-1} are assigned to the A′ WCH bending and A″ WH_2 deformation mode, while the deuterium counterparts are not observed due to their low frequencies. The observed absorptions correlate with the calculated values for CH≡WH_2Cl as shown in Table 9. Scale factors for the harmonic calculations given in Table 10 are slightly higher than for the analogous Mo complex. Again, anharmonic frequencies provide better agreement, particularly for the W−H stretching modes, but the W−H

TABLE 10: Comparison of Observed (Argon Matrix) and Calculated (DFT) Harmonic and Anharmonic Frequencies for the $CH{\equiv}WH_2Cl$ and $CH{\equiv}WH_2Br$ Complexes[a]

$CH{\equiv}WH_2Cl$				$CH{\equiv}WH_2Br$				
observed	harm B3LYP	harm BPW91	anharm B3LYP	observed	harm B3LYP	harm BPW91	anharm B3LYP	mode descript
1926.2	1996.1(0.965)[b]	1964.3(0.981)[b]	1902.2(1.013)[b]	1924.1	1994.7(0.965)[b]	1961.8(0.981)[b]	1904.8(1.010)[b]	A′ WH_2 str.
1921.4	1990.1(0.965)	1960.5(0.980)	1893.6(1.015)	1919.5	1989.1(0.965)	1958.3(0.980)	1895.8(1.013)	A″ WH_2 str.
766.8	788.5(0.972)	802.5(0.956)	758.4(1.011)	766.4	786.8(0.974)	800.0(0.958)	734.6(1.043)	A′ WH_2 bend.
697.2	728.1(0.958)	704.8(0.989)	699.9(0.996)	697.4	728.1(0.958)	705.2(0.989)	712.4(0.979)	A′ WH_2 wag
612.2	639.2(0.958)	621.8(0.985)	617.7(0.991)	*c*	634.9	619.4	628.2	A′ WCH bend
602.0	620.6(0.970)	607.4(0.991)	594.0(1.013)	*c*	616.3	604.5	603.0	A″ WH_2 def

[a] All calculations used 6-311++G(3df,3pd)/SDD basis set, and all frequencies are in cm^{-1}. Observed in an argon matrix. Description gives major coordinate. [b] Scale factors (observed/calculated frequencies). [c] Overlapped by precursor band.

stretching frequencies are now calculated 1% too low. We note that this is a fate also shared with anharmonic frequency calculations for the water molecule.[26b]

W + CH_3Br. The W + CH_3Br spectra shown in Figures 5 and 6 are very similar to the spectra of W + CH_3Cl. The II absorption at 1888.5 cm^{-1} and its deuterium counterpart at 1353.5 cm^{-1} (H/D ratio of 1.395) are almost undoubtedly the W−H stretching bands of $CH_2{=}WHBr$. The absorption at 853.4 cm^{-1} showing a D shift of −88.2 cm^{-1} (H/D ratio of 1.115) is assigned to the mixed C=W stretching mode. The band at 663.6 cm^{-1} has its D counterpart at 517.5 cm^{-1} (H/D ratio of 1.282) and is attributed to the CH_2 wagging mode. Harmonic calculations predict these fequencies as described above (Table 8), but the anharmonic frequencies are 1% low for the W−H stretch, a larger 3% too high for the wag, and 22 cm^{-1} too low for the mixed C=W mode, which shows that the standard anharmonic calculation fails to correctly model lower-frequency motions. The III absorptions at 1924.1 and 1919.5 cm^{-1} with their D counterparts at 1379.5 and 1377.4 cm^{-1} (H/D ratios of 1.395 and 1.394) are due to the antisymmetric and symmetric WH_2 stretching bands of $CH{\equiv}WH_2Br$. The absorptions at 766.4 and 697.4 cm^{-1} show D shifts of −212.0 and −157.5 cm^{-1} (H/D ratios of 1.382 and 1.292) and are assigned to the WH_2 bending and wagging modes as supported by the harmonic frequency calculations in Table 9. The harmonic calculations give frequencies that are a few percent higher, as for the chlorine derivative, and again, the anharmonic calculations predict the W−H stretching frequencies 1% too low. The WH_2 bending mode is the most difficult mode to model in all calculations (Table 10).

The relative intensities of the III absorptions to those of the II absorptions are higher in the W + CH_3Br spectra than in the W + CH_3Cl spectra as shown in Figure 5. In fact, the III absorptions are weakest relative to the II absorptions in the W + CH_3F spectra, suggesting that the methylidyne complex becomes relatively more favored with increasing halogen size. It is notable that a reverse trend is observed in the Mo systems, as described above. It is not clear at the moment what causes the difference. Previous studies show that the higher oxidation-state complex is more favored energetically for the heavier metal.[4−10] The transition state for conversion of the methylidene complex to the corresponding methylidyne complex via α-hydrogen migration perhaps becomes more stable with increasing halogen size, due to increased electron density in the carbon−metal bond. This may lead to more production of the methylidyne complex for the third-row transition metals with increasing halogen size.

Molecular Structures. The Mo and W reaction product structures calculated using B3LYP/6-311++G(3df,3pd)/SDD are shown in Figures 7 and 8, and the molecular parameters including those of the single insertion complexes are listed in Tables S1, S2, and S3. The Mo and W methylidene complexes in fact show the most agostic distortions among the early

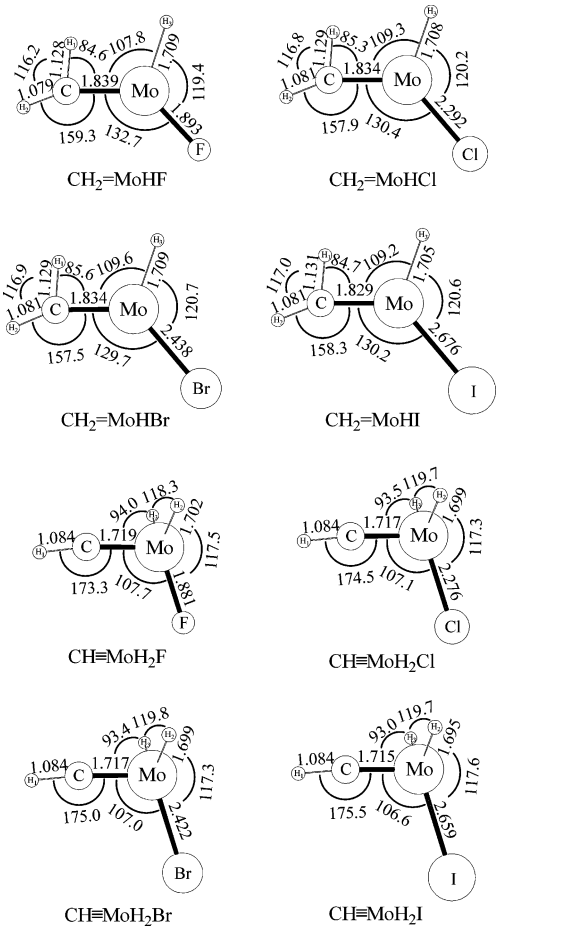

Figure 7. The optimized molecular structures of the $CH_2{=}MoHX$ and $CH{\equiv}MoH_2X$ calculated using B3LYP and 6-311++G(3df,3pd) for nonmetal atoms and SDD for metal atoms, except the SDD pseudopotential and basis are used for I. The bond lengths and angles are in Å and deg, respectively.

transition-metal methylidene complexes recently provided in reactions of laser-ablated metal atoms with methyl halides.[4−6] Analogous BPW 91 calculations give similar results with slightly more agostic distortion for the Mo and W methylidenes. The present and previous results indicate that the agostic distortion increases with increasing atomic number in the same row: group 3 metal methylidene complexes show essentially no agostic distortion.[33] Recent studies of small methylidene complexes formed from metal atoms and methyl halides indicate that more electron density in the carbon−metal bond normally leads to more agostic distortion.[4−6] The current results show that more valence electrons on the metal atom with increasing atomic number in the same row eventually result in more agostic interaction. We have noted the relativisitic effect in the increased W−H stretching frequencies in the methylidene complexes

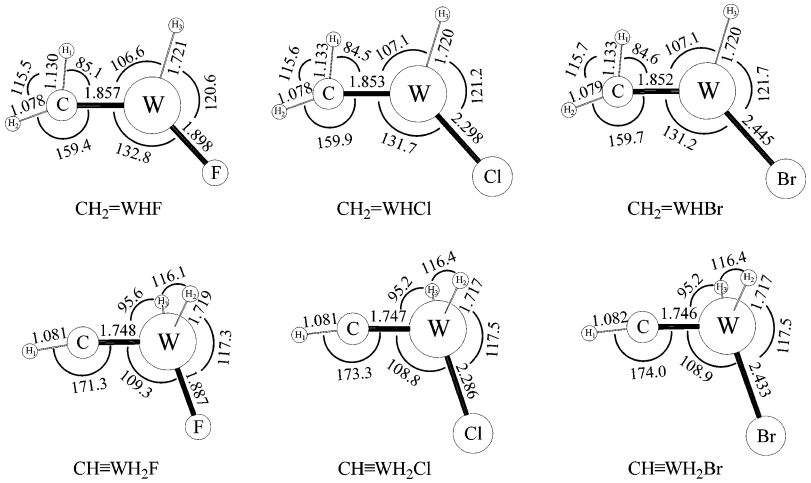

Figure 8. The optimized molecular structures of the $CH_2{=}WHX$ and $CH{\equiv}WH_2X$ calculated using B3LYP and 6-311++G(3df,3pd)/SDD. The bond lengths and angles are in Å and deg, respectively. Note that the C−W bond length decreases with increasing halogen size for both the methylidene and methylidyne complexes, indicating that increasing electron density of the metal atom leads to a stronger C−W bond.

relative to the corresponding Mo−H frequencies.[31] However, our DFT calculations reveal slightly longer W=C and W−H bonds than the Mo counterparts, but slightly smaller H−C=W angles for Cl and Br but not for the F substituent. It is interesting to consider if there is a relativistic effect on the agnostic interaction, and we suggest that higher-level structure calculations should be done to search for this possibility.

Agostic interactions were originally described as occuring due to an attraction between the electron-deficient metal center and the C−H bond acting as a Lewis base.[14] The agostic bond forms at the expense of a significant distortion within the ligand including bending at CH_2 and lengthening of the C−H bond. Alternatively, Scherer and McGrady suggested in a recent work that the agostic interaction arises from negative hyperconjugation delocalization of the carbon−metal bonding electrons rather than the donation of electron density locate on the alkyl substituent into a vacant orbital of the electron deficient metal atom.[15] Therefore, the agostic interaction includes not just the inclination of the C−H bond toward the d^0-metal atom but rearrangement of the molecular structure around the carbon−metal bond. More recently, it is also reported in studies for groups 4 and 5 metal methylidene complexes formed from laser-ablated metal atoms and methyl halides that the carbon−metal bond becomes shorter with increasing halogen size, while the C=M stretching frequency increases and the complex is more agostically distorted.[4,5]

Figures 7 and 8 also show that the carbon−metal bond lengths decrease with increasing halogen size for both the methylidene and methylidyne complexes, in line with previous results for groups 4 and 5 metal systems. The lower electronegativity with increasing halogen size most likely allows more electron density to remain in the carbon−metal bond and, as a result, leads to a stronger carbon−metal bond.

However, the ligand effects on agostic distortion and carbon−metal stretching frequency in the group 6 methylidene complexes are not consistent. The W methylidene complexes shown in Figure 8 become more agostically distorted with increasing halogen size, consistent with the groups 4 and 5 systems; however, a reverse trend is observed from the Mo methylidene complexes (except $CH_2{=}MoHI$) in Figure 7. The observed carbon−metal stretching frequencies also show conflicting trends; the highest C=M stretching frequency is observed from $CH_2{=}MoHCl$ among the Mo complexes, whereas the frequency is almost unaffected by the halogen ligand for the W complexes. For group 6 metal methylidenes, variation in electron density of the carbon−metal bond caused by the halogen ligand is apparently not the only major factor that determines the magnitude of agostic distortion and the carbon−metal stretching frequency.

Conclusions

Reactions of laser-ablated Mo and W atoms with methyl halides in excess argon have been carried out during condensation at 8 K. Two primary products, the methylidene and methylidyne complexes, are responsible for the two sets of absorptions observed in the infrared spectra. Visible photolysis ($\lambda > 420$ nm) converts the methylidene complex ($CH_2{=}MHX$) to the methylidyne complex ($CH{\equiv}MH_2X$) via α-hydrogen migration, whereas UV photolysis ($240 < \lambda < 380$ nm) reverses the effect. The present results show that the smallest possible methylidyne complexes are formed readily regardless of halogen size, while the Mo and W methylidynes are slightly less and more favored relative to the methylidene complexes with increasing halogen size, respectively.

The methylidene complexes are predicted to be the most agostically distorted among the groups 3−6 metal complexes provided from laser-ablated metal atoms and methyl halides, probably because more valence electrons of the group 6 metals allow higher electron density in the carbon−metal bond. While the carbon−metal bond length decreases with increasing halogen size, consistent with previous results, contrasting tendencies are found for the magnitudes of agostic distortion and the carbon−metal stretching frequencies of the Mo and W methylidenes. This suggests that there are other important factors regarding the agostic interaction and C=M stretching frequency of the group 6 metal methylidenes, in addition to the electron density in the carbon−metal bond.

B3LYP calculations predict harmonic frequencies 2−5% higher than argon matrix values, while computed anharmonic frequencies are only 1−2% higher for Mo−H stretching modes and 1−3% higher for the more difficult to model bending modes. However, the calculated anharmonic frequencies are the opposite: 1−2% lower for W−H stretching modes and 2% lower to 4% higher for metal hydride bending modes than the observed argon matrix values. Thus, calculating frequencies for Mo and W methylidene and methylidyne complexes is not an exact science, but very good approximations are obtained to support the experimental assignments for these new molecules.

Acknowledgment. We gratefully acknowledge financial support from NSF grant CHE 03-52487 to L.A.

Supporting Information Available: Tables S1, S2, and S3 of geometrical parameters and physical constants. This material is available free of charge via the Internet at http://pubs.acs.org.

References and Notes

(1) (a) Schrock, R. R. *J. Am. Chem. Soc.* **1975**, *97*, 6577. (b) Schrock, R. R. *J. Am. Chem. Soc.* **1974**, *96*, 6796. (c) McLain, S. J.; Wood, C. D.; Messerle, L. W.; Schrock, R. R. *J. Am. Chem. Soc.* **1978**, *100*, 5962.

(2) (a) Schrock, R. R. *Chem. Rev.* **2002**, *102*, 145. (b) Buchmeiser, M. R. *Chem. Rev.* **2000**, *100*, 1565.

(3) Tran, E.; Legzdins, P. *J. Am. Chem. Soc.* **1997**, *119*, 5071.

(4) (a) Cho, H.-G.; Andrews, L. *J. Phys. Chem. A* **2004**, 108, 6294. (Ti + CH_3F). (b) Cho, H.-G.; Andrews, L. *Inorg. Chem.* **2005**, *44*, 979 (Ti + CH_3X). (c) Cho, H.-G.; Andrews, L. *J. Am. Chem. Soc.* **2004**, *126*, 10485 (Zr + CH_3F). (d) Cho, H.-G.; Andrews, L. *Organometallics* **2004**, *23*, 4357 (Hf + CH_3F). (e) Cho, H.-G.; Andrews, L. *Chem. Asian J.*, in press (Zr, Hf + CH_3X).

(5) (a) Cho, H. G.; Andrews, L. *Organometallics* **2006**, *25*, 477 (Nb + CH_3F). (b) Cho, H. G.; Andrews, L. *J. Phys. Chem. A* **2006**, *110*, 10063.(V, Nb, and Ta + CH_3X).

(6) (a) Cho, H.-G.; Andrews, L. *Chem.—Eur. J* **2005**, *11*, 5017 (Mo + CH_3F). (b) Cho, H. G.; Andrews, L. *Organometallics* **2005**, *24*, 5678 (Cr, W + CH_3F).

(7) (a) Andrews, L.; Cho, H.-G.; Wang, X. *Inorg. Chem.* **2005**, *44*, 4834 (Ti + CH_4). (b) Cho, H.-G.; Wang, X.; Andrews, L. *Organometallics* **2005**, *24*, 2854 (Hf + CH_4). (c) Andrews, L.; Cho, H.-G.; Wang, X. *Angew. Chem., Int. Ed.* **2005**, *44*, 113 (Zr + CH_4). (d) Cho, H.-G.; Wang, X.; Andrews, L. *J. Am. Chem. Soc.* **2005**, *127*, 465 (Zr + CH_4).

(8) Cho, H. G.; Andrews, L. *J. Phys. Chem. A* **2006**, *110*, 3886 (V, Nb, and Ta + CH_4)

(9) (a) Cho, H.-G.; Andrews, L. *J. Am. Chem. Soc.* **2005**, *127*, 8226 (Mo + CH_4). (b) Cho, H.-G.; Andrews, L.; Marsden, C. *Inorg. Chem.* **2005**, *44*, 7634 (Cr, W + CH_4).

(10) Andrews, L.; Cho, H.-G. *Organometallics* **2006**, *25*, 4040 (review article).

(11) Siegbahn, P. E. M.; Blomberg, M. R. A. *Organometallics* **1994**, *13*, 354.

(12) Cundari, T. R.; Gordon, M. S. *J. Am. Chem. Soc.* **1992**, *114*, 539.

(13) (a) Franci, M. M.; Pietro, W. J.; Hout, R. F., Jr.; Hehre, W. J. *Organometallics* **1983**, *2*, 281. (b) Franci, M. M.; Pietro, W. J.; Hout, R. F., Jr.; Hehre, W. J. *Organometallics* **1983**, *2*, 815. (c) Dobbs, K. D.; Hehre, W. J. *J. Am. Chem. Soc.* **1986**, *108*, 4663.

(14) (a) Ujaque, G.; Cooper, A. C.; Maseras, F.; Eisenstein, O.; Caulton, K. G. *J. Am. Chem. Soc.* **1998**, *120*, 361. (b) Wada, K.; Pamplin, C. B.; Legzdins, P.; Patrick, B. O.; Tsyba, I.; Bau, R. *J. Am. Chem. Soc.* **2003**, *125*, 7035.

(15) Scherer, W.; McGrady, G. S. *Angew. Chem., Int. Ed.* **2004**, *43*, 1782.

(16) von Frantzius, G.; Streubel, R.; Brandhorst, K.; Grunenberg, J. *Organometallics* **2006**, *25*, 118.

(17) (a) Zhou, M. F.; Andrews, L. *J. Phys. Chem. A* **1998**, *102*, 8251. (b) Andrews, L.; Citra, A. *Chem. Rev.* **2002**, *102*, 885, and references therein. (c) Wang, X.; Andrews, L. *J. Phys. Chem. A* **2003**, *107*, 570.

(18) Kudin, K. N.; Burant, J. C.; Millam, J. M.; Iyengar, S. S.; Tomasi, J.; Barone, V.; Mennucci, B.; Cossi, M.; Scalmani, G.; Rega, N.; Petersson, G. A.; Nakatsuji, H.; Hada, M.; Ehara, M.; Toyota, K.; Fukuda, R.; Hasegawa, J.; Ishida, M.; Nakajima, T.; Honda, Y.; Kitao, O.; Nakai, H.; Klene, M.; Li, X.; Knox, J. E.; Hratchian, H. P.; Cross, J. B.; Adamo, C.; Jaramillo, J.; Gomperts, R.; Stratmann, R. E.; Yazyev, O.; Austin, A. J.; Cammi, R.; Pomelli, C.; Ochterski, J. W.; Ayala, P. Y.; Morokuma, K.; Voth, G. A.; Salvador, P.; Dannenberg, J. J.; Zakrzewski, V. G.; Dapprich, S.; Daniels, A. D.; Strain, M. C.; Farkas, O.; Malick, D. K.; Rabuck, A. D.; Raghavachari, K.; Foresman, J. B.; Ortiz, J. V.; Cui, Q.; Baboul, A. G.; Clifford, S.; Cioslowski, J.; Stefanov, B. B.; Liu, G.; Liashenko, A.; Piskorz, P.; Komaromi, I.; Martin, R. L.; Fox, D. J.; Keith, T.; Al-Laham, M. A.; Peng, C. Y.; Nanayakkara, A.; Challacombe, M.; Gill, P. M. W.; Johnson, B.; Chen, W.; Wong, M. W.; Gonzalez, C.; Pople, J. A. *Gaussian 03*, revision B.04, Gaussian, Inc.: Pittsburgh, PA, 2003.

(19) (a) Becke, A. D. *J. Chem. Phys.* **1993**, *98*, 5648. (b) Lee, C.; Yang, Y.; Parr, R. G. *Phys. Rev. B* **1988**, *37*, 785.

(20) Frisch, M. J.; Pople, J. A.; Binkley, J. S. *J. Chem. Phys.* **1984**, *80*, 3265.

(21) Andrae, D.; Haeussermann, U.; Dolg, M.; Stoll, H.; Preuss, H. *Theor. Chim. Acta* **1990**, *77*, 123.

(22) Zhou, M. F.; Andrews, L.; Bauschlicher, C. W., Jr. *Chem. Rev.* **2001**, *101*, 1931.

(23) Jacox, M. E. *Chem. Phys.* **1994**, *189*, 149.

(24) Korsgen, H.; Urban, W.; Brown, J. M. *J. Chem. Phys.* **1999**, *110*, 3861.

(25) Chertihin, G. V.; Andrews, L. *J. Phys. Chem.* **1995**, *99*, 1214.

(26) (a) Barone, V. *J. Chem. Phys.* **2004**, *120*, 3059. (b) Barone, V. *J. Chem. Phys.* **2005**, *122*, 014108. (c) Page, M.; Doubleday: C.; McIver, J. W., Jr. *J. Chem. Phys.* **1990**, *93*, 5634.

(27) Wang, X.; Andrews, L. *J. Phys. Chem. A* **2005**, *109*, 9021.

(28) Scott, A. P.; Radom, L. *J. Phys. Chem.* **1996**, *100*, 16502.

(29) Andersson, M. P.; Uvdal, P. L. *J. Phys. Chem. A* **2005**, 109, 3937.

(30) (a) Jensen, E. T. *J. Chem. Phys.* **2005**, *123*, 204709. (b) Okada, S.; Ohoyama, H.; Kasai, T. *J. Chem. Phys.* **2003**, *119*, 7131.

(31) (a) Pyykko, P.; Desclaux, J. P. *Chem. Phys. Lett.* **1977**, *50*, 503. (b) Pyykko, P.; Snijders, J. G.; Baerends, E. *J. Chem. Phys. Lett.* **1981**, *83*, 432. (c) Ziegler, T.; Snijders, J. G.; Baerends, E. J. *J. Chem. Phys.* **1981**, *74*, 1271. (d) Pyykko, P. *Chem. Rev.* **1988**, *88*, 563.

(32) (a) Wang, X.; Andrews, L. *J. Phys. Chem. A* **2002**, *106*, 6720. (b) Wang, X.; Andrews, L. *J. Am. Chem. Soc.* **2002**, *124*, 5636.

(33) Cho, H.-G.; Andrews, L. Unpublished data (Sc, Y, La + CH_3X).